RSC Pharmaceutics

ROYAL SOCIETY OF CHEMISTRY

PAPER

View Article Online
View Journal | View Issue

Cite this: *RSC Pharm.*, 2026, **3**, 136

Development of vismodegib-loaded PLGA nanoparticles for the treatment of pancreatic cancer: formulation and *in vitro* assessment in co-culture monolayers and spheroids

Ubah Abdi, Minao Zhang and Wafa T. Al-Jamal *

The desmoplastic tumour microenvironment (TME) is a defining feature of pancreatic cancer and serves as a major barrier to drug delivery and efficacy. Vismodegib is a clinically approved drug that targets the Hedgehog pathway *via* its receptor, Smoothened. This pathway is activated in cancer-associated fibroblasts (CAFs), one of the main cell types in the TME. In this study, vismodegib was loaded into PLGA nanoparticles to improve its solubility and enhance the efficacy of the chemotherapeutic drug gemcitabine. Vismodegib-loaded PLGA nanoparticles (Vis-PLGA NPs) were prepared and optimised based on PLGA polymer, drug to polymer ratio and formulation method. Vis-PLGA NPs formulated by the single emulsion method improved the encapsulation efficiency from 36% to 86% when compared to nanoprecipitation. More importantly, the drug release profile demonstrated a slower burst release, with sustained release for the single emulsion method at 35% *vs.* 86% for nanoprecipitation after 48 h. In pancreatic stellate cells, Vis-PLGA NP treatment selectively inhibited 2D co-cultured-induced Hh pathway activation *via* the effector glioma-associated protein 1 (Gli1) when compared to free vismodegib. More importantly, Vis-PLGA NPs enhanced gemcitabine efficacy as a sequential treatment by prolonging spheroid growth inhibition, combined with a higher apoptotic cell population compared to gemcitabine single treatment (10.3% *vs.* 7.5%). This increase in apoptosis was not observed with free vismodegib pre-treatment compared to gemcitabine alone. These promising results provide a platform for further *in vitro* characterisation and *in vivo* studies of Vis-PGLA NPs for pancreatic cancer treatment.

Received 15th June 2025,
Accepted 6th October 2025

DOI: 10.1039/d5pm00161g

rsc.li/RSCPharma

1. Introduction

Pancreatic ductal adenocarcinoma (PDAC) is a leading cause of cancer mortality globally, with 5-year survival rates of around 5%.[1] A characteristic feature of PDAC is the desmoplastic tumour microenvironment (TME) that contributes to disease progression and drug resistance.[2] A major stromal cell type of the TME is cancer-associated fibroblasts (CAFs), which are responsible for the desmoplastic reaction observed in pancreatic cancer.[3]

The activation of CAFs in the TME is due to aberrant Hedgehog (Hh) pathway activation *via* ligand-dependent paracrine signalling between tumour and stromal cells.[4] Sonic Hedgehog (SHh) ligands are secreted by tumour cells and bind to the Patched receptor in stromal cells to relieve the inhibition of Smoothened. This results in the activation of the pathway *via* the effector Gli1 and transcription of downstream target genes.[5] In response, stromal cells secrete growth factors that enhance tumour cell growth.[6] This has made the Hh pathway a therapeutic target to normalise the TME and address therapeutic resistance. This could also sensitise the tumour for subsequent treatment.[7]

Vismodegib is a clinically approved drug administered orally for the treatment of basal-cell carcinoma (BCC) and was discovered by high-throughput screening of a small molecule compound library.[8] It inhibits the Hh pathway by binding to the receptor SMO, thus preventing the activation of Hh target genes.[9] The efficacy of the drug was first determined in an Hh-dependent cancer model in which vismodegib produced complete tumour regression.[10] It has since been investigated for use in other cancer types, including pancreatic cancer, but with limited success in clinical trials.[11–13] Vismodegib is poorly water soluble, a major limiting factor for its bioavailability. One way researchers have looked at addressing this is by using NPs as a drug delivery system to improve the therapeutic efficacy of vismodegib.[14] For example, Karaca *et al.* used polymeric micelles for the co-delivery of vismodegib and gemcitabine and found a synergistic effect, with the downregulation of Hh markers Ptch and Gli1, inhibition of tumour

School of Pharmacy, Queen's University Belfast, 97 Lisburn Road, Belfast, BT9 7BL, UK. E-mail: w.al-jamal@qub.ac.uk

growth in a xenograft model and the suppression of epithelial–mesenchymal transition.[15] Vismodegib has been loaded into a range of lipid-based or polymeric nanoparticles.[15–21]

Poly(lactic-*co*-glycolic) acid (PLGA) is an FDA-approved polymer that has been extensively investigated due to its biodegradable and biocompatible nature. A co-polymer of polylactic acid (PLA) and poly-glycolic acid (PGA), PLGA, degrades in water by hydrolysis to its component monomers.[22] Nanoparticles (NPs) using PLGA have been widely used as a drug delivery system for therapeutic agents, particularly for cancer treatment.[23] The use of PLGA nanoparticles for hydrophobic drugs can improve bioavailability and allow controlled drug delivery and release.[24,25] PLGA polymers possess the intrinsic properties of their monomers, which affect the final NP formulation.[26] For example, by increasing the amount of PLA and thus the ratio of LA : GA, the PLGA polymer becomes more hydrophobic, slowing the degradation rate and thus drug release.[27] Furthermore, the properties of PLGA can be modified with end-chain modifications, such as ester end-capping or a more hydrophilic, acid-terminated PLGA, which can delay degradation considerably.[28] This provides an opportunity to control the NP drug release profile based on the polymer.

In this study, vismodegib-loaded PLGA NPs (Vis-PLGA NPs) were prepared and optimised based on the selected parameters of PLGA type, drug to polymer ratio and two formulation methods: nanoprecipitation and single emulsion (Fig. 1). The physicochemical properties, drug loading and release were determined, and efficacy was assessed in 2D and 3D models. Our results demonstrated that the single emulsion method was the best for Vis-PLGA NP preparation, improving encapsulation efficiency and drug release when compared to nanoprecipitation. In pancreatic stellate cells, Vis-PLGA NPs selectively inhibited 2D co-culture-induced Hh activation. Furthermore, in a 3D spheroid model of pancreatic cancer and pancreatic stellate cells, Vis-PLGA NP pre-treatment enhanced the growth inhibition observed for gemcitabine single treatment, with a greater induction of apoptosis. This was not observed with free vismodegib pre-treatment with gemcitabine in the spheroids. The present study emphasises the importance of formulation parameters and supports further research on vismodegib treatment using nanoparticles to improve therapeutic efficacy for pancreatic cancer.

2. Materials and methods

2.1. Materials

Vismodegib and gemcitabine were purchased from MedChemExpress (Sollentuna, Sweden). Poly(DL-lactic-*co*-glycolic acid) (PLGA) (5002, 5002A, 5004, 5004A, 7502, 7502A) was kindly gifted by Corbion (Amsterdam, Netherlands). Poly(vinyl alcohol) (M_w 13 000–23 000, 87–89% hydrolysed), acetonitrile HPLC Plus, ≥99.9%, dichloromethane HPLC Plus, ≥99.8%, methanol HPLC Plus, ≥99.9%, sodium chloride ACS reagent,

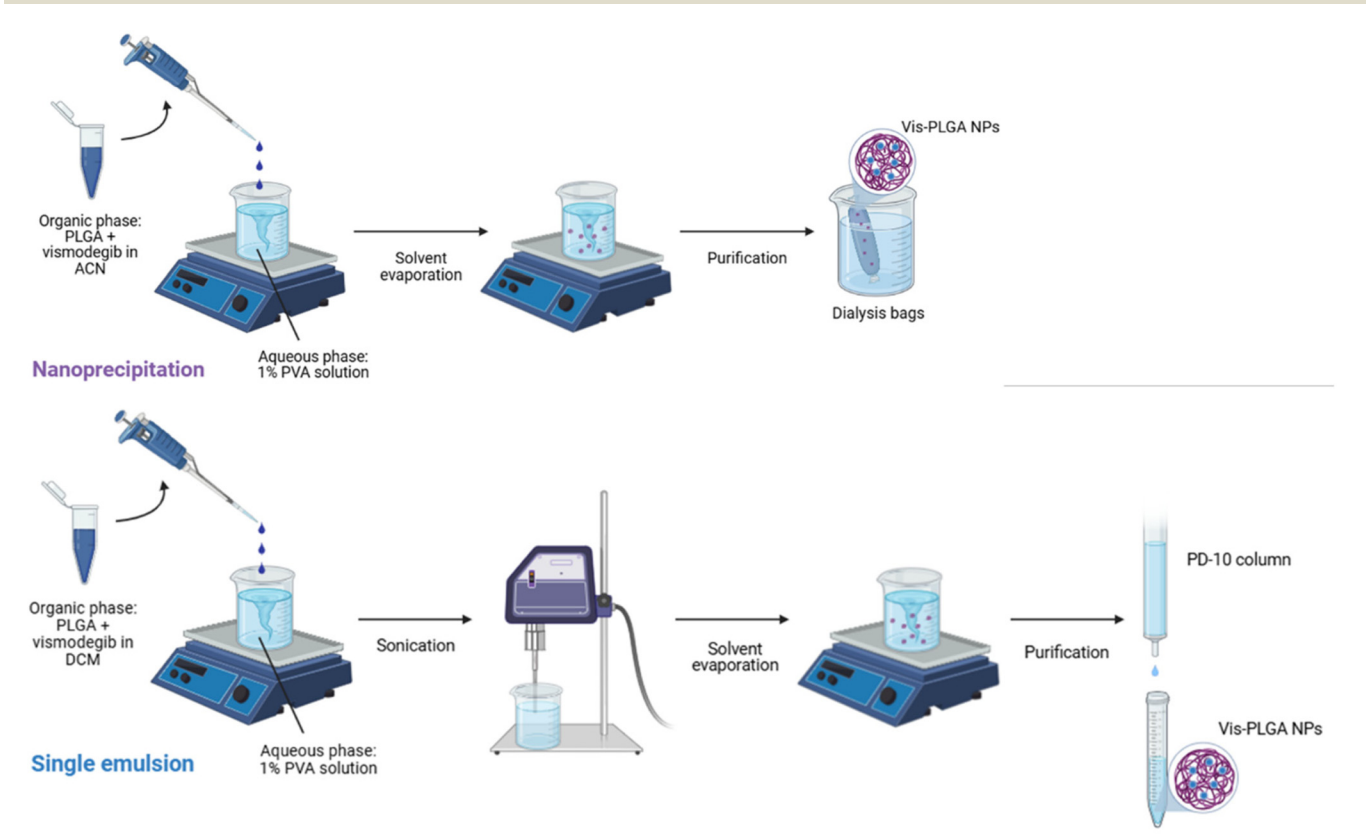

Fig. 1 Schematic of the nanoprecipitation and single emulsion methods used to formulate the Vis-PLGA NPs.

methyl cellulose, agarose, Nile red, resazurin sodium salt, phosphate buffered saline (PBS), and heat-inactivated foetal bovine serum (FBS) were purchased from Sigma-Aldrich (Dorset, UK). Phosphoric acid, for HPLC 85%–90%, Roswell Park Memorial Institute medium (RPMI), Dulbecco's Modified Eagle Medium (DMEM), Dulbecco's PBS (DPBS), 0.25% trypsin-EDTA phenol red solution, penicillin–streptomycin (10 000 U mL^{-1}), sodium pyruvate (100 mM), dimethyl sulfoxide (DMSO) and Hoechst 33342 were purchased from Thermo Fisher Scientific (Cheshire, UK). Flat bottom 96-well plates, round bottom 96-well plates, flat bottom 6-well plates, and tissue culture inserts for 6-well plates (PET, transparent, pore size: 0.4 μm) were purchased from Sarstedt Ltd (Leicester, UK).

2.2. Preparation of vismodegib-loaded PLGA NPs using nanoprecipitation

PLGA polymer types used for the formulation of vismodegib-loaded PLGA NPs are summarised below (Table 1). Briefly, PLGA polymer (6.67 mg) was dissolved in 1 mL of acetonitrile and then added to 500 μL of 4 mg mL^{-1} of vismodegib in acetonitrile. This solution was then added dropwise to 2 mL of 1% PVA solution while stirring on a magnetic stirrer at 350 rpm and stirred overnight at room temperature. The resulting solution of NPs was then purified using dialysis tubing with a 10 kDa molecular weight cut-off (Thermo Scientific, UK) in deionised water for 24 h.

2.3. Preparation of vismodegib-loaded PLGA NPs using the single emulsion method

PLGA polymer 7502A (6.67 mg) was dissolved in 1 mL of dichloromethane and then added to 500 μL of 4 mg mL^{-1} of vismodegib in dichloromethane. This was added dropwise to 2 mL of 1% PVA solution while stirring on a magnetic stirrer at 350 rpm at room temperature. The sample was then sonicated for 2 or 3 minutes at 50% amplitude using the Model 120 Sonic Dismembrator (Fisher Scientific, UK) on ice and left to stir at 350 rpm overnight at room temperature. Nanoparticles were purified using a PD-10 column, in which 2.5 mL of the sample was loaded into the column pre-washed with PBS. The first flow through was discarded, and 3.5 mL of PBS was used to elute the purified sample.

2.4. Physicochemical characterisation of vismodegib-loaded PLGA NPs

The hydrodynamic diameter, polydispersity and zeta-potential of the NPs were measured using dynamic light scattering with the Zetasizer Nano ZS90 (Malvern Panalytical, UK). For each measurement, 1 mL of the sample was prepared by diluting the NPs (1 : 10) with 10 mM sodium chloride or water when the samples were in water or PBS. Disposable cuvettes (Fisher Scientific, UK) were used for size and polydispersity, and disposable folded capillary cells (Malvern Panalytical, UK) were used for zeta-potential. At least 3 runs were performed for each triplicate measurement.

Table 1 Composition of the PLGA polymer types used in the present study

PLGA type	Lactide: glycolide ratio	Molecular weight (kg mol^{-1})	Inherent viscosity (dl g^{-1})
5002A	50:50	14	0.2
5004A	50:50	44	0.4
7502A	75:25	17	0.2

2.5. Transmission electron microscopy (TEM) characterisation

TEM images were taken using a JEOL JEM-1400 plus high contrast transmission electron microscope, at an accelerating voltage of 120 kV. Samples were prepared by depositing a drop of the NPs previously filtered through a 0.45 μm filter on a carbon-coated 300 mesh TEM copper grid (3.05 mm, TAAB, UK) and left to air-dry at room temperature in a fume hood.

2.6. Determination of vismodegib encapsulation efficiency and drug loading using high performance liquid chromatography (HPLC)

For the extraction of vismodegib from the nanoparticles, the samples were diluted (1 : 20) in acetonitrile, followed by 30 minutes of sonication. After allowing the polymer to precipitate, the supernatant was then collected, and the amount of vismodegib was quantified by HPLC.

The 1260 Infinity II HPLC system (Agilent, UK) was used to quantify the concentration of vismodegib. 10 μL of sample was injected into the ZORBAX Eclipse Plus Phenyl-Hexyl column (4.6 × 100 mm, 5 μm, Agilent UK) for 5 minutes at room temperature at a flow rate of 0.6 mL min^{-1}. The mobile phase was a mixture of 0.05% phosphoric acid solution and acetonitrile at a ratio of 45 : 55. An isocratic method was used, and UV detection was set at 262 nm. Measurements were performed in triplicate and are shown as mean ± standard deviation.

Vismodegib encapsulation efficiency (EE, %) and drug loading (DL, %) were determined using eqn (1) and (2), respectively:

$$\mathrm{EE}\,(\%) = \frac{\text{encapsulated drug}\,(\mu g)}{\text{initial drug}\,(\mu g)} \times 100, \quad (1)$$

$$\mathrm{DL}\,(\%) = \frac{\text{encapsulated drug}\,(\mu g)}{\text{initial PLGA}\,(\mu g)} \times 100. \quad (2)$$

2.7. *In vitro* drug release study for Vis-PLGA NPs

1 mL of vismodegib-loaded PLGA NPs at 100 μg mL^{-1} in PBS was added to dialysis bags (10 kDa MCWO, ThermoFisher Scientific, UK) and immersed in 20 mL of PBS containing Tween 80 (0.2%, v/v) buffer. The samples were then incubated at 37 °C under agitation at 100 rpm in a water bath. At each time point, 1 mL of the PBS-Tween 80 buffer was collected and replaced with an equivalent volume of PBS-Tween 80 each time. The samples were then quantified by HPLC with an

injection volume of 40 μL, as described above. Cumulative drug release was determined using eqn (3):

$$\text{Cumulative vismodegib release (\%)} = \frac{([V_t] \times 20\,\text{mL}) + [V_{t-1}] + [V_{t-2}] + \cdots}{[V_s]} \times 100, \quad (3)$$

where $[V_t]$ is the concentration of vismodegib at the selected time point, $[V_{t-1}]$ is the concentration of vismodegib at the time point previous to t and $[V_s]$ is the initial concentration of vismodegib.

2.8. Preparation of fluorescently labelled Nile red PLGA nanoparticles for *in vitro* uptake studies

PLGA polymer 7502A (6.67 mg) was dissolved in 1 mL of dichloromethane and then added to 500 μL of 0.625 mg mL^{-1} of Nile red in methanol, followed by the single emulsion method and PD-10 column purification, as described earlier. For quantification, Nile red was extracted from the purified nanoparticles using methanol (1 : 20 dilution) and 30 minutes of sonication. Nile red encapsulation efficiency and drug loading in purified NPs were determined by measuring the fluorescence intensity (λ_{ex} = 544 nm, λ_{em} = 620–10 nm) of Nile red NPs using a FLUOstar Omega plate reader (BMG Labtech, UK) with a standard curve prepared from 0.01–1 mg mL^{-1} Nile red in methanol.

2.9. Cell culture maintenance

The imPSC cells were kindly provided by Professor Angela Mathison (Medical College, Wisconsin, USA), and the KPC cells were kindly provided by Professor Jennifer Morton (Beatson Institute for Cancer Research, UK). imPSC cells were cultured in DMEM, with high glucose supplemented with 10% heat-inactivated FBS and 100 units per mL penicillin–streptomycin, and KPC cells were cultured under the same conditions as imPSC but with the additional supplement of 1 mM sodium pyruvate. All cell lines were routinely grown in a standard T-75 cm^2 cell culture flask and maintained in a cell culture incubator at 37 °C and 5% CO_2. Cells were passaged regularly upon reaching 70%–80% confluency to maintain cells within the exponential growth phase. For passaging and cell detachment, the cell culture medium was removed from the flasks, and adherent cells were rinsed with 4 mL of DPBS containing no calcium and no magnesium. Then, 1 mL of 0.25% Trypsin-EDTA solution was added to the flask, and the cells were incubated at 37 °C until cell detachment was observed under an inverted light microscope. To deactivate the trypsinisation, 9 mL of complete cell culture medium was added, and cells were split at the desired cell density.

2.10. Vismodegib/Vis-PLGA NP toxicity assessment in single culture pancreatic cell lines using the resazurin assay

KPC (1×10^4 cells per well) and imPSC (1.5×10^4 cells per well) were seeded in 96-well plates with complete cell culture medium and allowed to attach overnight. The following day, the medium was removed and replaced with different concentrations of vismodegib or Vis-PLGA NPs diluted in complete medium and incubated for 24–72 h. Cells treated with 10% DMSO were used as a positive control for cell toxicity. After incubation, cell viability was determined using the resazurin assay, where mitochondrial activity in live cells reduced resazurin to fluorescent resorufin. Drug and/or NP containing media were replaced with fresh cell culture media containing 0.01 mg mL^{-1} resazurin and incubated for 4 h in a cell culture incubator at 37 °C and 5% CO_2. Following resazurin incubation, 150 μL of the media was transferred to black 96-well plates, and the fluorescence intensity (λ_{ex} = 544 nm, λ_{em} = 590 nm) was measured using a FLUOstar Omega plate reader (BMG Labtech, UK). Wells containing media with 0.01 mg mL^{-1} resazurin were used as the blank group. Cell viability was calculated by normalisation to the untreated control group using eqn (4):

$$\text{Cell viability (\%)} = \frac{\text{fluorescence of treated group} - \text{fluorescence of blank group}}{\text{fluorescence of control group} - \text{fluorescence of blank group}}. \quad (4)$$

2.11. Indirect co-culture using transwell plates

An indirect co-culture of pancreatic cancer and stellate cells was established using transwell plates. KPC cells (7.5×10^4 cells) were seeded on the insert membrane (0.4 μm, Sarstedt Ltd), and imPSC cells (1.5×10^5 cells) were seeded into the well of a 6-well plate and incubated at 37 °C and 5% CO_2 for 72 h.

2.12. Characterisation of Gli1 protein expression by western blot

For co-cultured imPSC, the cells were incubated as an indirect co-culture, as described above. After incubation, the cells were collected and lysed using an RIPA lysis buffer solution containing protease inhibitors (1 : 100 dilution). The total protein concentration was then determined using the Pierce™ BCA protein assay kit. Next, 30 μg of protein was separated by SDS-PAGE using a 10% polyacrylamide gel and transferred onto a polyvinylidene difluoride (PVDF) membrane (0.45 μm pore size, Sigma-Aldrich, UK). The membrane was then blocked for 1 h with 5% (w/v) milk in TBS buffer with 0.1% Tween 20 (TBS-T) and then incubated with an anti-Gli1 antibody (1 : 1000 dilution, MA532553, Life Technologies Ltd) at 4 °C overnight. The membrane was washed in TBS-T three times and then incubated with a secondary antibody conjugated with horseradish peroxidase (HRP) (1 : 3000 dilution, 7074S, Cell Signalling Technology) at room temperature for 1 h. After washing, the bands were visualized using enhanced chemiluminescence. β-Actin expression (1 : 1000, 4967S, Cell Signalling Technology) was used as an internal loading control.

2.13. Characterisation of Gli1 mRNA expression by qPCR

Total RNA was extracted from the co-cultured imPSC cells using the Purelink RNA Mini kit (Thermo Fisher, #12183018A)

following the manufacturer's instructions. To quantify the concentration and purity of the extracted RNA, the Nanodrop 2000 spectrophotometer (ThermoFisher Scientific, UK) was used to determine the 260/280 and 260/230 nm ratios. The extracted RNA was then reverse transcribed to cDNA using the Superscript IV First-Strand Synthesis System kit according to the manufacturer's instructions. Real-time quantitative PCR was performed using the LightCycler 480 SYBR Green I kit and detected using the LightCycler 480 system (Roche Ltd, UK). Pre-designed Gli1 primers were purchased from Origene (#MP205464), with GAPDH(#MP205604) used as the internal control. mRNA expression was presented as fold change compared to the untreated control after normalisation to the internal control, GAPDH, using the $2^{-\Delta\Delta Ct}$ method.

2.14. Pancreatic spheroid formation

A stock solution in media was first prepared by weighing 6 g of methyl cellulose and autoclaving at 121 °C for 30 minutes. Next, 250 mL of serum free DMEM media was pre-heated to 60 °C for 30 minutes, added to the methyl cellulose powder and left to stir at 60 °C for 20 minutes on a hotplate stirrer. Then, 250 mL of DMEM media containing 20% FBS at room temperature was added to the mixture and left to stir at 4 °C overnight. The final solution was centrifuged at 5000*g* for 2 h at room temperature, and only the clear and highly viscous supernatant was collected and aliquoted for storage at −20 °C for long-term storage (around 95% of the stock solution). For spheroid formation, an aliquot of the stock solution was pre-heated at 37 °C before use. Next, KPC and imPSC cells were co-cultured at 1500 total cells per well (1 : 2 ratio) in 80% complete cell culture media and 20% methyl cellulose stock solution in round bottom 96-well plates. This corresponds to a final concentration of 0.24% (w/v) methyl cellulose in DMEM media. The cell culture medium was changed every 3–4 days by removing 100 μL spent media and replacing it with 100 μL fresh media. The growth of the spheroids was monitored over 13 days by measuring the spheroid diameter using the Cell3iMager imaging system (SCREEN, USA).

2.15. Sequential treatment of vismodegib/Vis-PLGA NPs, followed by gemcitabine in spheroids

KPC + imPSC spheroids were cultured using methyl cellulose, as described above. For combination treatment, spheroids with an approximate diameter of 600 μm (on day 4) were treated with 20 μM and 50 μM vismodegib or Vis-NPs and 100 nM gemcitabine for 48 h by removing 100 μL of cultured media and replacing it with the drug or NP at double the desired final concentration. For sequential treatment, KPC + imPSC spheroids were pre-treated with 20 μM and 50 μM vismodegib or Vis-NPs for 48 h, and the treatment was removed. The spheroids were then treated with 100 nM gemcitabine for a further 48 h, and growth was monitored.

2.16. Apoptosis assay in spheroids

KPC + imPSC spheroids were pre-treated with 50 μM vismodegib or Vis-NPs for 48 h, followed by 100 nM gemcitabine for another 48 h. KPC + imPSC spheroids were collected for dissociation into single cells. After sedimentation of the spheroids, the supernatant was removed, and the spheroids were incubated with 0.25% Trypsin-EDTA at 37 °C for 5 min. During this time, the spheroids were vortexed and resuspended using a pipette to encourage dissociation. After achieving single cells, complete media was added to deactivate Trypsin, and the cells were washed with PBS. Apoptosis was assessed using the eBioscience™ Annexin V-FITC Apoptosis Detection Kit. Briefly, cells were resuspended in 1× Binding Buffer at 5×10^5 cells per mL, and 5 μL of Annexin V-FITC was added to 195 μL of cell suspension. The cells were mixed and incubated at room temperature for 10 minutes before washing and resuspending in 1× Binding Buffer. Finally, 10 μL of propidium iodide (PI) (20 μg mL^{-1}) was added to 190 μL cell suspension before flow cytometry analysis using the BD FACSCalibur flow cytometer (Becton Dickinson, USA). Annexin V-FITC fluorescence for apoptotic cells was detected using the FL-1 detector, and PI fluorescence for necrotic cells was detected using the FL-3 detector. 10 000 events were obtained for each sample, and data analysis was performed using FlowJo software (FlowJo, USA).

2.17. Statistical analysis

All statistical tests and graphing were completed using GraphPad Prism 8.0 (GraphPad Software, USA). Data are presented as mean ± standard deviation (SD). Statistical significance between groups was determined using either a Student's *t* test, one-way analysis of variance (ANOVA) or two-way ANOVA, followed by either a Dunnett's or Tukey's *post hoc* test.

3. Results

3.1. Preparation of Vis-PLGA NPs using nanoprecipitation

3.1.1. PLGA polymer type affects the physicochemical properties of Vis-PLGA NPs. The nanoprecipitation method was first applied to formulate PLGA nanoparticles using twelve different PLGA polymers. This was to determine the effect of molecular weight (PLGA 5002 *vs.* PLGA 5004), lactide:glycolide ratio (PLGA 5002 *vs.* PLGA 7502) and end-cap modification (PLGA 5002/5004/7502 *vs.* PLGA 5002A/5004A/7502A) on the physicochemical properties of the nanoparticles. PLGA polymers with acid-termination produced smaller nanoparticles than those with no end-cap modifications, with an average size of <150 nm as opposed to >200 nm for polymers with no modification (Table S1). When loading vismodegib into PLGA nanoparticles, a similar pattern was observed with acid-terminated PLGA polymers producing smaller nanoparticles (Tables 2 and S2). Vismodegib encapsulation efficiency was between 20% and 30% for all the polymers used (Tables 2 and S2). Therefore, smaller, acid-terminated PLGA types (PLGA 5002A, 5004A and 7502A) were used for further assessments of vismodegib loading.

3.1.2. Drug to polymer ratio affects the physicochemical properties and loading of Vis-PLGA NPs. Next, we examined

Table 2 Properties of vismodegib-loaded PLGA nanoparticles (Vis-PLGA NPs) prepared using nanoprecipitation and different lactide:glycolide ratios and molecular weights. Vis-PLGA NPs were prepared using the nanoprecipitation method and 1 mg of vismodegib. All PLGA polymers were acid-terminated, as denoted by the letter A. The hydrodynamic diameter, polydispersity index (PdI) and zeta-potential were determined using dynamic light scattering (DLS). Vismodegib encapsulation efficiency (EE) and drug loading (DL) were determined using HPLC. Data are shown as mean ± standard deviation (SD) (n = 3)

PLGA type	Hydrodynamic diameter ± SD (nm)	PdI ± SD	Zeta-potential ± SD (mV)	DL ± SD (%)	EE ± SD (%)
5002A	117.1 (± 1.6)	0.122(± 0.019)	−1.72 (± 0.25)	3.74 (± 0.24)	25.5 (± 1.8)
5004A	105.2 (± 1.4)	0.140 (± 0.038)	−2.18 (± 0.47)	3.18 (± 0.11)	22.9 (± 0.1)
7502A	141.4 (± 4.0)	0.127 (± 0.008)	−1.27 (± 0.19)	3.96 (± 0.12)	27.8 (± 0.9)

the effect of drug to polymer (w/w) ratios on the size, polydispersity and encapsulation efficiency of Vis-PLGA nanoparticles. The amount of vismodegib was fixed at 1 mg, and a drug to polymer (w/w) ratio ranging from 1 : 2 to 1 : 20 was assessed. For all polymers, lower drug to polymer ratios of 1 : 2–1 : 3 produced nanoparticles with highly polydisperse populations >0.3 and a low encapsulation efficiency of ≤13%. At higher ratios, smaller nanoparticles with low PdI were formed, and encapsulation efficiency increased to 35%–40%. Therefore, an initial optimal ratio of 1 : 6.7 was selected for all polymers (Table S3).

To improve the drug loading, the amount of vismodegib was doubled, resulting in a new drug to polymer (w/w) ratio of 1 : 3. When compared to the previous ratio, no real change was observed in the size or polydispersity of the nanoparticles. However, the encapsulation efficiency decreased for both Vis-PLGA 5002A NPs and Vis-PLGA 5004A NPs, with no increase in drug loading. Interestingly, the encapsulation efficiency for the Vis-PLGA 7502A NPs remained the same, while the drug loading doubled (Fig. 2B). Following this, the *in vitro* drug release profiles for Vis-PLGA 7502A and Vis-PLGA 5002A at the 1 : 3 drug to polymer ratio were assessed (Fig. 2C). Rapid drug release from both nanoparticles was observed within the first 2 hours, with vismodegib release at 77% for both nanoparticles compared to 56% for free vismodegib. This could indicate the rapid release of the loosely attached drug to the surface of the dialysed nanoparticles.

Due to the rapid drug release profile observed, with no difference between PLGA polymer types, the purification

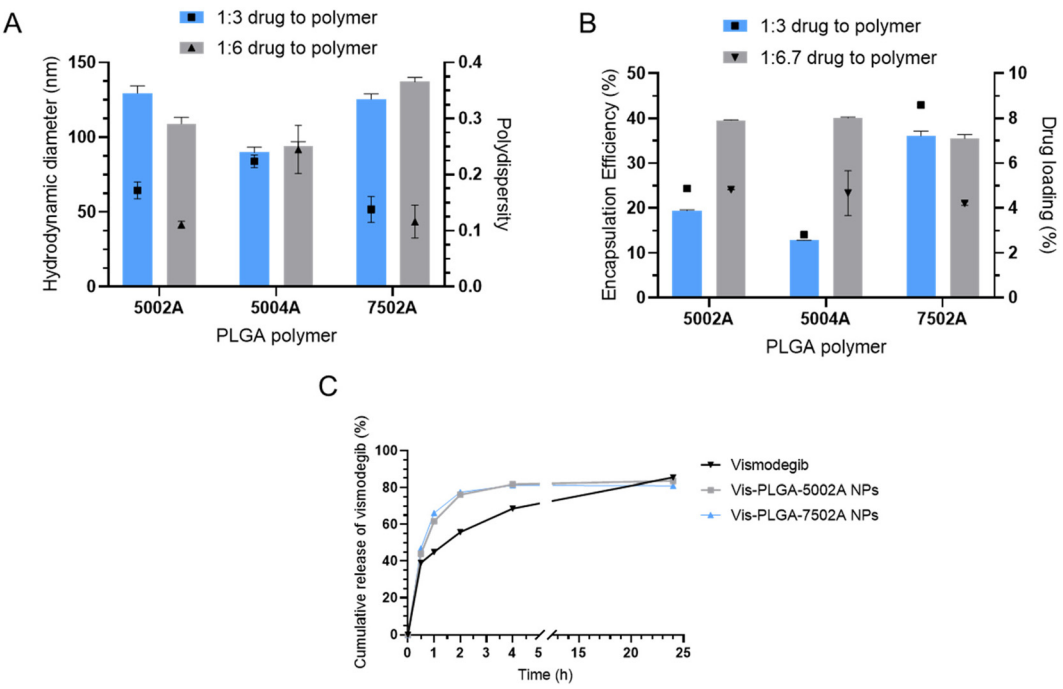

Fig. 2 Properties of vismodegib-loaded PLGA nanoparticles (Vis-PLGA NPs) prepared at a higher drug to polymer ratio (w/w). Vis-PLGA NPs were prepared using the nanoprecipitation method at 1 : 3 or 1 : 6.7 drug to polymer ratio (w/w) using PLGA 5002A, 5004A and 7502A. (A) The hydrodynamic diameter (bars) and polydispersity (symbols) were determined using dynamic light scattering (DLS). (B) Encapsulation efficiency (bars) and drug loading (symbols) were determined using HPLC. (C) The *in vitro* drug release profiles for Vis-PLGA 5002A and 7502A at 1 : 3 were assessed. Drug release was assessed using the dialysis method, where 100 μg mL^{-1} of Vis-PLGA NPs were prepared in PBS and placed into dialysis bags (MWCO 10 kDa). The bags were then immersed in 20 mL of PBS with 0.2% (v/v) Tween 80 and incubated at 37 °C under constant shaking. At each time point, 1 mL of release media was removed for analysis and replaced with fresh PBS with 0.2% (v/v) Tween 80. Drug release was determined using HPLC. Data are shown as mean ± standard deviation (SD) (n = 3).

method was changed from dialysis to PD-10 columns. However, a similar drug release profile was observed with vismodegib release at 68% within the first 2 hours, and 78% after 4 hours (data not shown). As this failed to improve the drug release profile, an alternative formulation method was investigated.

3.2. Preparation of Vis-PLGA NPs using single emulsion improves the drug release profile

The formulation method used for the preparation of PLGA NPs can affect the drug release profile, with the single emulsion method previously shown to slow down release.[29,30] Therefore, the single emulsion method was used to prepare Vis-PLGA nanoparticles at 2 sonication times (Fig. 3). Vis-PLGA 7502A NPs at both 1 : 3 and 1 : 6.7 were larger in size with a hydrodynamic size of >250 nm and polydispersity ranging from 0.2 and 0.4 (Fig. 3A). The encapsulation efficiency of Vis-PLGA 7502A NPs sonicated for 2 minutes ranged from 51% to 53%, with drug loading ranging from 5% to 12%. Sonicating for 3 minutes resulted in higher encapsulation ranging from 74% to 84% and drug loading ranging from 10% to 21% (Fig. 3C). Based on this, a sonication time of 3 minutes was selected, and the optimal formulation of Vis-PLGA 7502A at 1 : 3 was used to determine the drug release profile (Fig. 3D). Vismodegib release was slower than the free drug, with 22% drug release observed within the first hour. A sustained drug

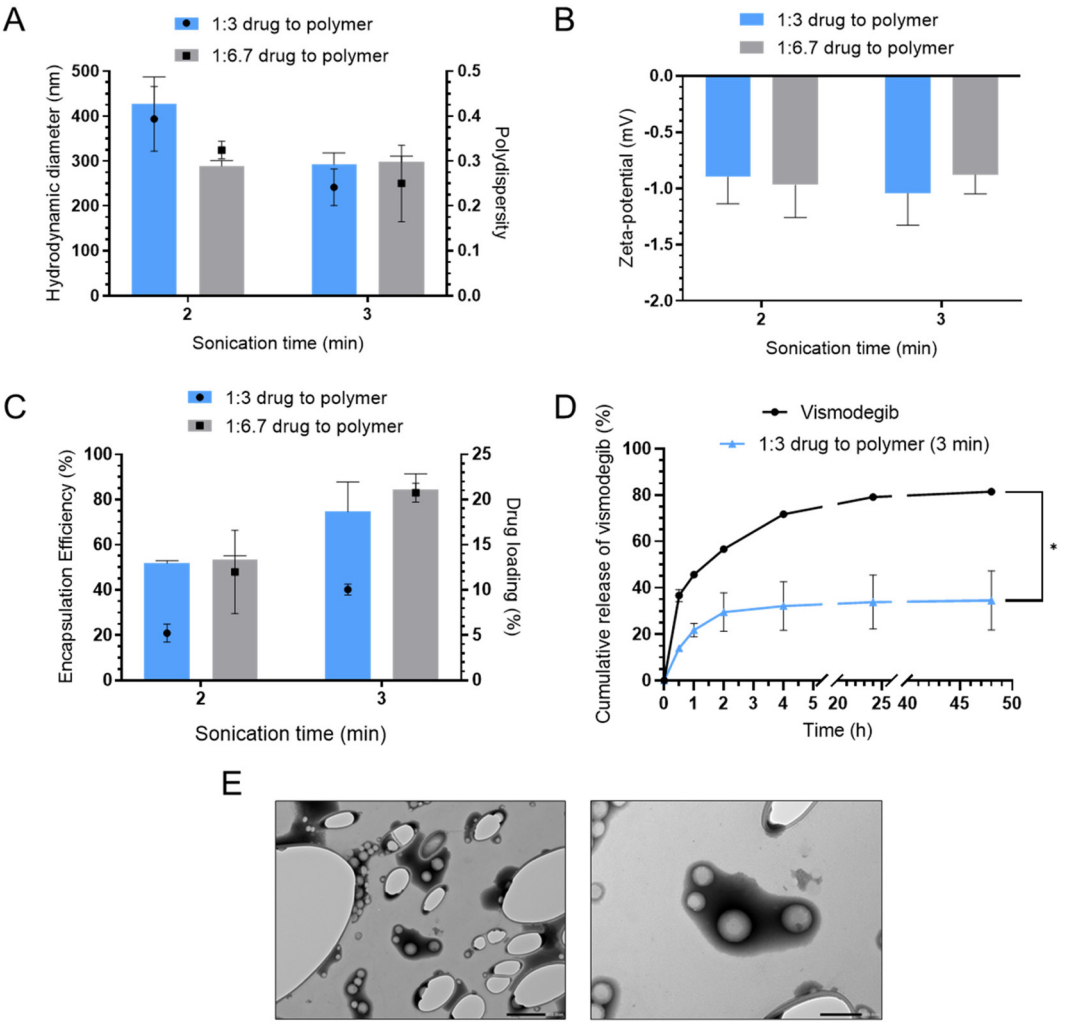

Fig. 3 Preparation of Vis-PLGA NPs using the single emulsion method. Vis-PLGA NPs (7502A) were prepared by single emulsion at 1 : 3 and 1 : 6.7 drug to polymer ratio (w/w), changing the time of sonication. (A) The hydrodynamic diameter (bars), polydispersity (symbols) and (B) zeta-potential were determined using dynamic light scattering (DLS). (C) Vismodegib encapsulation (bars) and drug loading (symbols) were determined using HPLC. Data are shown as mean ± standard deviation (n = 3). (D) Drug release profile of Vis-PLGA 7502A NPs at a drug to polymer ratio of 1 : 3 and continuous sonication of 3 minutes. Drug release was assessed using the dialysis method, where 100 μg mL^{-1} of the Vis-PLGA NPs were prepared in PBS and placed into dialysis bags (MWCO 10 kDa). The bags were then immersed in 20 mL of PBS with 0.2% (v/v) Tween 80 and incubated at 37 °C under constant shaking. At each time point, 1 mL of release media was removed for the analysis and replaced with fresh PBS with 0.2% (v/v) Tween 80. (E) Transmission electron microscope micrographs of the optimised Vis-PLGA NP formulation. Scale bar: 500 nm (left) and 200 nm (right). Drug release was determined using HPLC. Data are shown as mean ± standard deviation (n = 3). Statistical analysis was performed using the Student's t-test (*p < 0.05).

release was achieved after 2 hours, with vismodegib release at 35% after 48 hours. Thus, this was selected as the best NP formulation for the Vis-PLGA nanoparticles. The morphology of the optimised Vis-PLGA NPs was also characterised using transmission electron microscopy (TEM) (Fig. 3E). Vis-PLGA NPs exhibited a spherical structure, with a diameter of ~ 160 nm, which is smaller than the hydrodynamic size determined by DLS, as reported by others.[31–33] The difference in particle size might be attributed to the dried vacuum state used for TEM *versus* the hydrodynamic size in the DLS.

The optimised Vis-PLGA NPs formulated by the nanoprecipitation and single emulsion techniques were then directly compared (Fig. 4). Vis-PLGA NPs formulated by nanoprecipitation produced smaller particles of 126 nm *vs.* 298 nm for single emulsion (Fig. 4A). The single emulsion method improved encapsulation from 36% to 86% and resulted in the highest drug loading at 23% (Fig. 4C). Finally, the drug release profile demonstrated a slower burst release for the single emulsion NPs, with release at 35% *vs.* 86% for nanoprecipitation after 48 hours (Fig. 4D). Vis-PLGA NPs formulated by the single method were then used for *in vitro* screening.

3.3. Vis-PLGA NP efficacy in murine pancreatic cell lines

Next, the cytotoxicity of Vis-PLGA NPs was determined in pancreatic cell lines using a resazurin assay. The murine pancreatic cancer line, KPC, and the pancreatic stellate cell line, imPSC, were treated with 20–50 μM vismodegib or Vis-PLGA NPs for 48 hours. In both cell lines, a similar toxicity profile was observed between the free vismodegib and Vis-PLGA NPs, with no reduction in cell viability (top and bottom of Fig. 5A). Targeting of the Hh pathway was then assessed in imPSC cells co-cultured with KPC using transwell plates for an indirect co-culture. When looking at the mRNA expression of the Hh pathway's effector, Gli1, no difference in expression was observed after vismodegib treatment. However, treatment with Vis-PLGA NPs resulted in downregulation of Gli1 mRNA expression, with a two-fold decrease observed at 20 and 50 μM (Fig. 5B). Furthermore, Gli1 protein expression after Vis-PLGA NP treatment resulted in downregulation at 50 μM (Fig. 5C and D). Promisingly, these results demonstrate enhanced Hh targeting of Vis-PLGA NPs over free vismodegib in a 2D co-culture setting.

3.4. Assessing the uptake of fluorescently labelled PLGA NPs in murine pancreatic cancer spheroids

Before assessing the efficacy of Vis-PLGA NPs in 3D *in vitro* models, the uptake of PLGA nanoparticles was investigated in murine pancreatic spheroids. This was done using a 3D co-culture spheroid model that successfully incorporated both KPC and imPSC cells, as previously developed in our group (Fig. S2).[34] Fluorescently labelled PLGA nanoparticles were first prepared by single emulsion using the fluorescent dye,

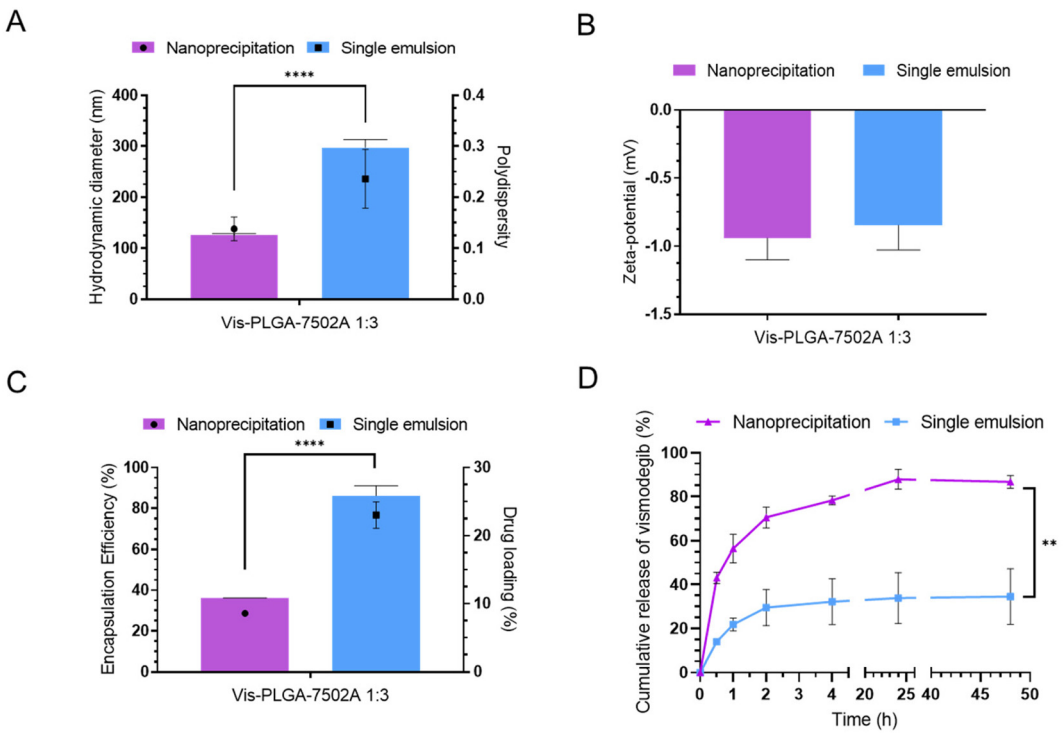

Fig. 4 Comparison of Vis-PLGA NPs prepared using nanoprecipitation *vs.* single emulsion. The best formulation for both nanoprecipitation and single emulsion was compared directly for (A) the hydrodynamic diameter (bars), polydispersity (symbols), and (B) zeta-potential determined by dynamic light scattering. (C) Vismodegib encapsulation efficiency (bars), drug loading (symbols) and (D) drug release profile were quantified using HPLC and were also compared. Data are shown as mean ± standard deviation (n = 3). Statistical analysis was performed using the Student's t-test (**p < 0.01, ***p < 0.001, and ****p < 0.0001 for hydrodynamic diameter, encapsulation efficiency and drug release).

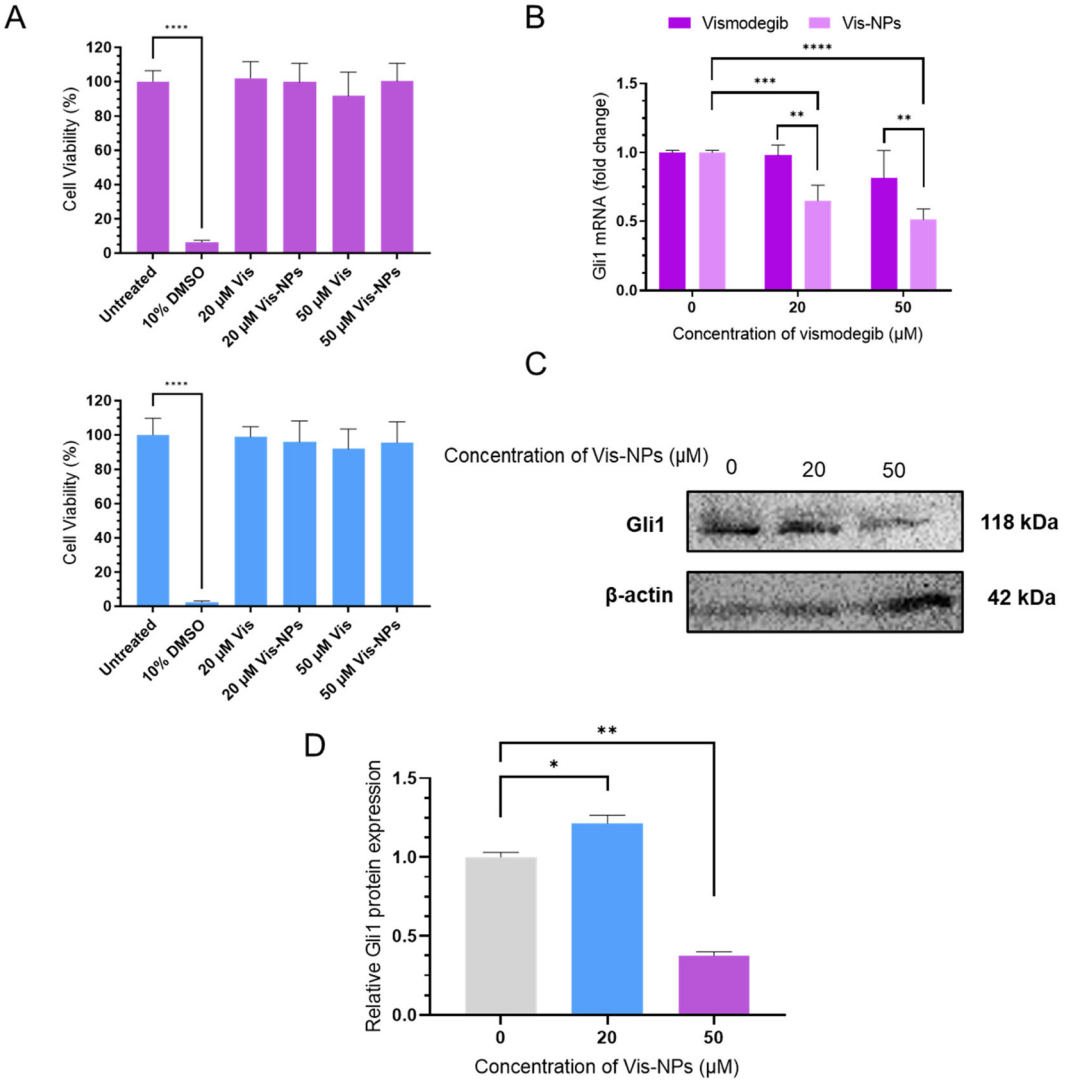

Fig. 5 Vis-PLGA NP treatment resulted in the downregulation of Gli1 mRNA expression in co-cultured imPSC cells. (A) KPC (top) and imPSC (bottom) cells were treated with 0–50 μM vismodegib and Vis-PLGA NPs (Vis-NPs) for 48 h. 10% DMSO was used as a positive toxicity control. The cell viability was then quantified by a resazurin assay and normalised to the untreated control cell group. (B) The mRNA expression of the Hedgehog pathway effector Gli1 was determined using RT-qPCR. The mRNA expression of Gli1 in imPSC cells co-cultured with KPC using transwell plates for 3 days, followed by 48 h treatment with 0–50 μM vismodegib and Vis-NPs. The results are shown as fold change to the untreated control group after normalisation to the internal control gene, GAPDH. (C and D) Expression of Gli1 was determined using western blot in imPSC cells co-cultured with KPC as described for mRNA expression and treated with Vis-NPs for 48 h. β-Actin was used as an internal control. Data are shown as mean ± SD from three independent experiments. Statistical analysis was determined using one-way ANOVA, followed by Tukey's multiple comparisons test comparing treated groups to the untreated control group for cell viability and western blot. A two-way ANOVA using Tukey's multiple comparisons test comparing every group's mean with every other mean for mRNA expression (**$p < 0.01$, ***$p < 0.001$, and ****$p < 0.0001$).

Nile red. Next, the spheroids were incubated with the fluorescently labelled PLGA NPs for 1–24 h, and uptake was assessed by fluorescent imaging using the Cytation 5 imaging reader. Uptake of the NPs was observed as early as 1 h and was still visible after 24 h (Fig. 6).

3.5. Vis-PLGA NP efficacy in murine pancreatic spheroids

After confirming uptake of the NPs in the 3D model, Vis-PLGA NP efficacy was investigated in combination with the clinically relevant chemotherapeutic drug, gemcitabine. This was to assess whether Vis-PLGA NP treatment could enhance gemcitabine toxicity as a combination or sequential treatment. KPC + imPSC spheroids were either treated with vismodegib or Vis-PLGA NPs at 50 μM combined with 100 nM gemcitabine for 48 hours (known as a combination treatment) or pre-treated with vismodegib or Vis-PLGA NPs at 50 μM for 48 hours, followed by 100 nM gemcitabine for 48 hours (known as a sequential treatment).

Spheroids treated with vismodegib or Vis-PLGA NPs in combination with gemcitabine demonstrated a similar growth

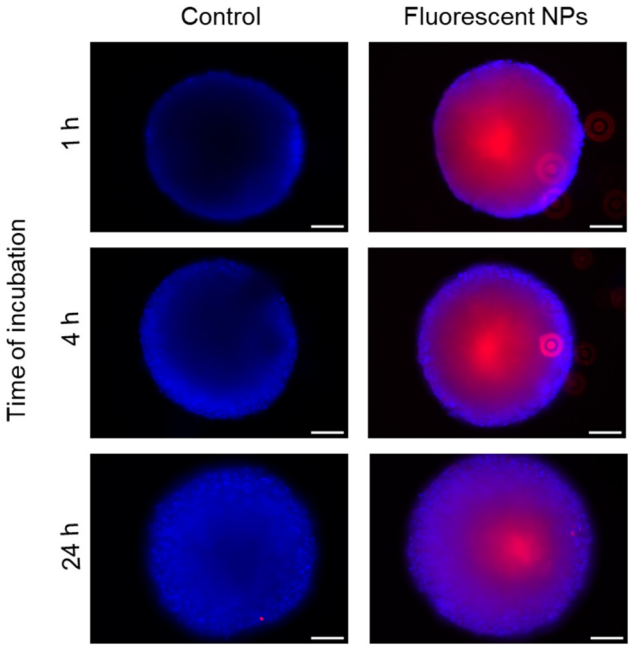

Fig. 6 PLGA NP uptake in 3D pancreatic spheroids. After 4 days of seeding, KPC + imPSC spheroids were incubated with or without 0.1 μg mL^{-1} Nile red-loaded PLGA nanoparticles (NPs) for 1–24 h, and uptake was determined using fluorescence imaging with the Cytation 5 microscope imager. The spheroids were also incubated with Hoechst 33342 (1 μg mL^{-1}) as a nuclear stain. Representative merged images are shown from the middle of the spheroid (at 180 μm) after 1–24 h incubation using DAPI and RFP filters (Ex/Em = 377/447 nm and 531/593 nm for each filter, respectively). Scale bar: 100 μm and taken at 10× magnification.

inhibition and recovery pattern to that observed with gemcitabine single treatment (Fig. 7A). For KPC + imPSC spheroids pre-treated with vismodegib or Vis-PLGA NPs, a prolonged inhibition of growth was observed when compared to gemcitabine treatment alone (Fig. 7B). Therefore, sequential treatment with Vis-PLGA NPs enhanced gemcitabine cytotoxicity in the KPC + imPSC spheroid model, and this condition was used to further investigate its efficacy. This was determined by assessing apoptosis using Annexin V and propidium iodide (PI) staining. After treatment, the spheroids were dissociated into single cells and stained with Annexin V-FITC and PI for flow cytometry analysis (Fig. 7C and D). The average total apoptotic (Annexin V positive) cell populations (Q2 + Q3) for spheroids treated with vismodegib or Vis-PLGA NPs alone were comparable to the untreated control population (4.1% (± 0.7%) and 5.6% (± 0.5%), respectively, *vs.* 4.9% (± 1.9%)). Gemcitabine single treatment significantly increased the apoptotic cell population to 7.5% (± 1.6%, $p = 0.002$). Interestingly, pre-treatment with Vis-PLGA NPs further increased the total apoptotic cell population to 10.3% (± 2.1%), which was significantly higher than that in the gemcitabine group ($p = 0.0070$) (Fig. 7C and D). This was not observed for pre-treatment with free vismodegib, where the total apoptotic cell population increased to only 7.3% (± 3.5%), similar to that of gemcitabine single treatment. This could be attributed to the prolonged release of vismodegib from the NPs.

4. Discussion

PLGA is a biocompatible polymer and a popular choice for nanoparticle formation. The properties of PLGA, such as lactide : glycolide ratio, molecular weight, inherent viscosity and end-capping, can all impact the formation and behaviour of NPs.[27] In this study, acid-terminated forms of three PLGA types were selected for the first time for the preparation of Vis-PLGA NPs. Acid-terminated Vis-PLGA NPs tended to form smaller particles compared to those with no end-cap modifications, with an average size of less than 150 nm (Table 2). Previous studies have shown that the presence of a charged group in PLGA polymers can affect the size and degradation of nanoparticles.[35] It is believed that during nanoparticle formation, charged particles enhance the nucleation rate and lead to the formation of smaller nanoparticles.[36] This highlights the importance of PLGA polymer properties on formulation parameters and was considered for this study.

The use of lower drug to polymer (w/w) ratios of 1 : 2–1 : 3 resulted in the formation of large and polydisperse particles. By increasing the polymer amount to increase the ratio, smaller particles formed a more monodisperse population. At the highest ratio, the particles were still monodispersed, but they increased in size (Table S3). Low amounts of PLGA can lead to unstable formation of particles, while higher amounts of PLGA can increase the viscosity of the organic phase and produce larger particles. This has been demonstrated previously in the literature for PLGA nanoparticles.[37,38] Thus, we chose the 1 : 6.7 drug to polymer ratio, which produced NPs < 150 nm and the highest loading of 35%–40%. Based on this, the polymer amount was fixed to prevent instability during nanoparticle formation, and vismodegib increased, resulting in a new drug to polymer (w/w) ratio of 1 : 3. This maintained most physicochemical properties of the NPs but doubled the drug loading for Vis-7502A NPs to 8%. This loading is similar to other vismodegib-loaded polymeric nanoparticles reported in the literature.[15,16,19,39,40] Kumar *et al.* developed polymeric micelles for co-delivery of vismodegib and miR-let7b for PDAC and achieved drug loading of 5%.[19] Wang *et al.* used polymeric pro-drug-based nanoparticles for vismodegib delivery, with drug loading at 5% and 12% depending on the block length.[16]

Unexpectedly, the release of vismodegib from Vis-PLGA NPs was rapid, with no difference between PLGA types (Fig. 2). A slower drug release profile was expected for PLGA 7502A due to its higher lactide:glycolide ratio, which increased hydrophobicity and decreased the degradation rate.[41] However, this was not the case with a similar release observed for PLGA 5002A. The rapid burst release we observed from our PLGA nanoparticles could be attributed to weakly bound or adsorbed drugs on the surface of the particles prepared *via* nanoprecipitation, with greater adsorption resulting in a larger burst effect.[42,43] Nevertheless, changing the purification method did

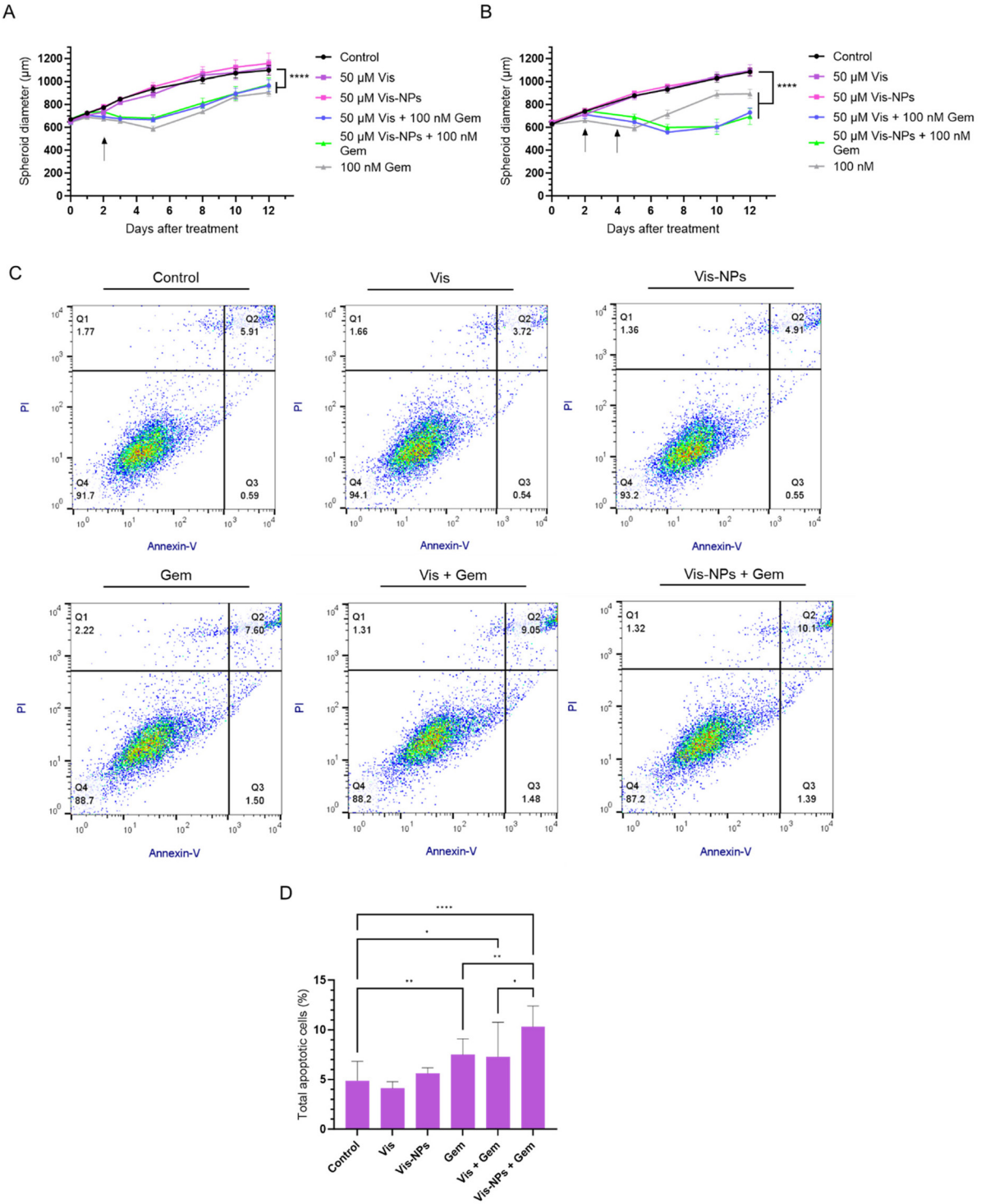

Fig. 7 Sequential treatment of Vis-PLGA NPs and gemcitabine prolongs growth inhibition and further induces apoptosis in KPC + imPSC spheroids. Growth curves of KPC + imPSC spheroids after (A) combination treatment with 50 μM vismodegib or Vis-NPs and 100 nM gemcitabine for 48 h or (B) sequential treatment of 50 μM vismodegib or Vis-NPs for 48 h, followed by 100 nM gemcitabine for 48 h on day 4 post seeding. Arrows indicate when vismodegib/Vis-NPs and gemcitabine treatments were removed. To assess apoptosis, KPC + imPSC spheroids were pre-treated with 50 μM vismodegib or Vis-NPs for 48 h, followed by 100 nM gemcitabine for 48 h on day 4 post seeding. Spheroids were then collected and dissociated into single cells before incubation with Annexin V-FITC and propidium iodide (PI) for the assessment of apoptosis with flow cytometry. (C) Representative scatter plots of KPC + imPSC spheroids following treatment. Q1 = necrotic cells, Q2 = late apoptotic cells, Q3 = early apoptotic cells and Q4 = viable cells. (D) Total percentage of Annexin V positive cells (Q2 + Q3) in KPC + imPSC spheroids after treatment. Data are shown as mean ± SD (n = 3). Statistical analysis was performed using a two-way ANOVA, followed by Tukey's multiple comparisons test comparing every group's mean with every other mean on day 12 for the growth curve. A one-way ANOVA, followed by Tukey's multiple comparisons test between all groups, was used for the total apoptotic cells (****p < 0.0001). (*p < 0.05, **p < 0.01, ***p < 0.001, and ****p < 0.0001).

not alter the drug release profile. Therefore, the single emulsion method was used to improve drug incorporation and delay its release, as reported by others.[44]

Nanoparticles formulated by the single emulsion method were larger in size, ranging from 250 to 300 nm in size with encapsulation nearly double that of what was achieved for nanoprecipitation (Fig. 4). Furthermore, increasing the sonication time increased Vis-PLGA NP loading without any effect on size or PdI. This is likely due to the higher sonication energy used overall to create the emulsion, resulting in increased drug loading.[45,46] It has also been shown that sonication affects the release rate of the drug due to the method of incorporation into NPs.[47,48] Accordingly, we managed to achieve a slower and sustained drug release profile using the single emulsion method with release at 86% *vs.* 35% for nanoprecipitation after 48 h. Wang *et al.* similarly reported slower release for PLGA nanoparticles loaded with salinomycin, where the release pattern of NPs prepared by nanoprecipitation was 89% for the first 24 h and 70% for those prepared by single emulsion.[29] A slower release profile was also observed with doxorubicin-loaded NPs.[30]

When determining Vis-PLGA NP efficacy *in vitro*, it was essential to consider *in vitro* models that incorporated the TME. This included the use of a 2D indirect co-culture of pancreatic cancer and stellate cells to allow for cell–cell interactions *via* secreted factors. In our study, Vis-PLGA NP treatment resulted in a significant downregulation of Gli1 mRNA and protein expression in co-cultured imPSC cells (Fig. 5B and C). This was not observed after free vismodegib treatment, confirming targeting with our Vis-PLGA NPs. Previous *in vitro* studies assessing vismodegib nanoparticles for pancreatic cancer have primarily focused on studying the Gli1 expression in cancer cells only.[15,16,19,20] Wang *et al.* used immortalised human pancreatic stellate cells *in vitro* and demonstrated Gli1 upregulation after an indirect co-culture with human pancreatic cancer cells, BxPC-3. However, they did not further assess the activity of vismodegib-loaded nanoparticles *in vitro*, focusing on an *in vivo* assessment similar to previous studies.[16] Therefore, the use of a 3D spheroid model representing the complex nature of PDAC can allow for further assessments, such as drug penetration and resistance *in vitro,* before the use of *in vivo* models.[49] We previously developed a murine 3D co-culture spheroid model for therapeutic screening.[34] In the present study, we also confirmed the uptake of fluorescently labelled PLGA NPs in these spheroids, making them a suitable model for testing Vis-PLGA NP efficacy (Fig. 6).

The complex and challenging nature of PDAC has pushed researchers to focus on targeting the pancreatic tumour microenvironment to improve therapeutic outcomes for patients. In particular, Hh pathway activation in CAFs produces a dense stromal reaction that impairs drug delivery and promotes chemoresistance.[50] Combination treatments with Hh inhibitors aim to improve drug delivery and improve therapeutic efficacy in pancreatic cancer.[51] Karaca *et al.* used polymeric micelle mixtures loading vismodegib for co-administration with gemcitabine for pancreatic cancer. These NPs induced apoptosis by upregulation of pro-apoptotic proteins and combination treatment with gemcitabine resulted in significant tumour growth inhibition.[15] Moreover, Wang *et al.* combined vismodegib treatment by loading the drug in SN38 (active metabolite of irinotecan) polymeric prodrug-based NPs. It was found that adding vismodegib to the treatment improved tumour growth inhibition in a dose-dependent manner and produced remarkable apoptotic induction in tumour tissues when compared to SN38 treatment alone.[16]

The treatment regimen is also important to consider and can further enhance the therapeutic efficacy of combined treatments.[52] Previous pre-clinical studies have demonstrated that pre-treatment with vismodegib can sensitise cancer to chemotherapeutic treatment.[53,54] Zhou *et al.* reported this in 2D indirect co-culture where vismodegib treatment reversed co-culture-induced doxorubicin resistance in SMO positive pancreatic cells.[53] However, our present study is the first to investigate pre-treatment using a 3D spheroid model of pancreatic cancer. Promisingly, sequential treatment of Vis-PLGA NPs with gemcitabine prolonged the inhibitory effect on the growth of the spheroids (Fig. 7A and B). This was not observed for the combination treatment, emphasising the importance of the dosing schedule for treatment. The sequential treatment with Vis-PLGA NPs also resulted in a significant increase in the total number of apoptotic cells when compared to gemcitabine single treatment, which was not observed for free vismodegib (Fig. 7C and D). This could likely be the cause of the prolonged inhibitory effect observed during the long-term assessment. These findings highlight the importance of using 3D models for therapeutic assessment, particularly when using drugs that target the tumour microenvironment.

5. Conclusion

In this study, we successfully prepared Vis-PLGA NPs with high encapsulation efficiency and a sustained drug release profile. The results demonstrate that the single emulsion method is better for Vis-PLGA NP formulation, improving the loading and drug release profile. In a 2D indirect co-culture, Vis-PLGA NPs selectively inhibited co-culture-induced Hh activation in pancreatic stellate cells when compared to free vismodegib. Furthermore, we demonstrated that Vis-PLGA NPs enhanced gemcitabine efficacy with prolonged growth inhibition during long-term assessment and greater induction of apoptosis when compared to vismodegib in a 3D co-culture spheroid model. These findings support further investigations *in vivo* of Vis-PLGA NPs to improve vismodegib tumour accumulation for the sensitisation of chemotherapeutic agents for pancreatic cancer.

Conflicts of interest

There are no conflicts to declare.

Data availability

The entire data generated and analysed during this study are included in the main manuscript and its supplementary information (SI). Supplementary information is available. See DOI: https://doi.org/10.1039/d5pm00161g.

Acknowledgements

The authors would like to thank the Department of Economy NI for funding this studentship. The authors would also like to thank Dr Chang Yang (Guizhou Medical University, China) for the PLGA nanoparticle formulation and HPLC training and Dr Ahlam Ali (University of Wolverhampton, UK) for PCR training.

References

1 A. Bengtsson, R. Andersson and D. Ansari, *Sci. Rep.*, 2020, **10**, 1–9.
2 J. A. G. Moir, J. Mann and S. A. White, *Surg. Oncol.*, 2015, **24**, 232–238.
3 Y. Sunami, J. Häußler, A. Zourelidis and J. Kleeff, *Cancers*, 2022, **14**, 744.
4 H. Tian, C. A. Callahan, K. J. Dupree, W. C. Darbonne, C. P. Ahn, S. J. Scales and F. J. De Sauvage, *Proc. Natl. Acad. Sci. U. S. A.*, 2009, **106**, 4254–4259.
5 D. Amakye, Z. Jagani, M. Dorsch, D. Amakye, Z. Jagani and M. Dorsch, *Nat. Med.*, 2013, **19**, 1410–1422.
6 A. M. Skoda, D. Simovic, V. Karin, V. Kardum, S. Vranic and L. Serman, *Biomol. Biomed.*, 2018, **18**, 8–20.
7 J. E. Cortes, R. Gutzmer, M. W. Kieran and J. A. Solomon, *Cancer Treat. Rev.*, 2019, **76**, 41–50.
8 S. E. Gould, J. A. Low, J. C. Marsters, K. Robarge, L. L. Rubin, F. J. De Sauvage, D. P. Sutherlin, H. Wong and R. L. Yauch, *Expert Opin. Drug Discovery*, 2014, **9**, 969–984.
9 S. Aditya and A. Rattan, *Indian Dermatol. Online J.*, 2013, **4**, 365–365.
10 G. J. P. Dijkgraaf, B. Alicke, L. Weinmann, T. Januario, K. West, Z. Modrusan, D. Burdick, R. Goldsmith, K. Robarge, D. Sutherlin, S. J. Scales, S. E. Gould, R. L. Yauch and F. J. De Sauvage, *Cancer Res.*, 2011, **71**, 435–444.
11 E. J. Kim, V. Sahai, E. V. Abel, K. A. Griffith, J. K. Greenson, N. Takebe, G. N. Khan, J. L. Blau, R. Craig, U. G. Balis, M. M. Zalupski and D. M. Simeone, *Clin. Cancer Res.*, 2014, **20**, 5937–5945.
12 D. V. T. Catenacci, M. R. Junttila, T. Karrison, N. Bahary, M. N. Horiba, S. R. Nattam, R. Marsh, J. Wallace, M. Kozloff, L. Rajdev, D. Cohen, J. Wade, B. Sleckman, H. J. Lenz, P. Stiff, P. Kumar, P. Xu, L. Henderson, N. Takebe, R. Salgia, X. Wang, W. M. Stadler, F. J. De Sauvage and H. L. Kindler, *J. Clin. Oncol.*, 2015, **33**, 4284–4292.
13 A. De Jesus-Acosta, E. A. Sugar, P. J. O'Dwyer, R. K. Ramanathan, D. D. Von Hoff, Z. Rasheed, L. Zheng, A. Begum, R. Anders, A. Maitra, F. McAllister, N. V. Rajeshkumar, S. Yabuuchi, R. F. de Wilde, B. Batukbhai, I. Sahin and D. A. Laheru, *Br. J. Cancer*, 2019, **122**, 498–505.
14 D. M. Valcourt, M. N. Dang, J. Wang and E. S. Day, *Ann. Biomed. Eng.*, 2019, 1–21, DOI: 10.1007/s10439-019-02399-7.
15 M. Karaca, R. Dutta, Y. Ozsoy and R. I. Mahato, *Mol. Pharm.*, 2016, **13**, 1822–1832.
16 L. Wang, X. Liu, Q. Zhou, M. Sui, Z. Lu, Z. Zhou, J. Tang, Y. Miao, M. Zheng, W. Wang and Y. Shen, *Biomaterials*, 2017, **144**, 105–118.
17 Y. Li, S. Pu, Q. Liu, R. Li, J. Zhang, T. Wu, L. Chen, H. Li, X. Yang, M. Zou, J. Xiao, W. Xie and J. He, *J. Controlled Release*, 2019, **303**, 77–90.
18 M. N. Calienni, D. M. Vega, C. F. Temprana, M. C. Izquierdo, D. E. Ybarra, E. Bernabeu, M. Moretton, F. C. Alvira, D. Chiappetta, S. D. V. Alonso, M. J. Prieto and J. Montanari, *Pharmaceutics*, 2021, **13**, 186–186.
19 V. Kumar, G. Mondal, P. Slavik, S. Rachagani, S. K. Batra and R. I. Mahato, *Mol. Pharm.*, 2015, **12**, 1289–1298.
20 P. Ray, M. Confeld, P. Borowicz, T. Wang, S. Mallik and M. Quadir, *Colloids Surf., B*, 2019, **174**, 126–135.
21 L. F. Zhang, W. Q. Deng, Q. W. Huang, J. J. Zhang, Y. Wang, T. J. Zhou, L. Xing and H. L. Jiang, *Adv. Mater.*, 2024, 2311474–2311474, DOI: 10.1002/ADMA.202311474.
22 H. K. Makadia and S. J. Siegel, *Polymers*, 2011, **3**, 1377–1397.
23 F. Danhier, E. Ansorena, J. M. Silva, R. Coco, A. Le Breton and V. Préat, *J. Controlled Release*, 2012, **161**, 505–522.
24 S. Acharya and S. K. Sahoo, *Adv. Drug Delivery Rev.*, 2011, **63**, 170–183.
25 S. Rezvantalab, N. I. Drude, M. K. Moraveji, N. Güvener, E. K. Koons, Y. Shi, T. Lammers and F. Kiessling, *Front. Pharmacol.*, 2018, **9**, 1260–1260.
26 P. Blasi, *J. Pharm. Invest.*, 2019, **49**, 337–346.
27 R. P. F. Lanao, A. M. Jonker, J. G. C. Wolke, J. A. Jansen, J. C. M. Van Hest and S. C. G. Leeuwenburgh, *Tissue Eng., Part B*, 2013, **19**, 380–390.
28 P. Gentile, V. Chiono, I. Carmagnola, P. V. Hatton, P. Gentile, V. Chiono, I. Carmagnola and P. V. Hatton, *Int. J. Mol. Sci.*, 2014, **15**, 3640–3659.
29 Q. Wang, P. Wu, W. Ren, K. Xin, Y. Yang, C. Xie, C. Yang, Q. Liu, L. Yu, X. Jiang, B. Liu, R. Li, L. Wang, Q. Wang, P. Wu, W. Ren, K. Xin, Y. Yang, C. Xie, C. Yang, Q. Liu, L. Yu, X. Jiang, B. Liu, R. Li and L. Wang, *Nanoscale Res. Lett.*, 2014, **9**, 1.
30 T. Jibowu, *J. Nanomed. Nanotechnol.*, 2016, **7**, 2.
31 B. K. Wilson and R. K. Prud'homme, *J. Colloid Interface Sci.*, 2021, **604**, 208–220.
32 X. Song, Y. Zhao, S. Hou, F. Xu, R. Zhao, J. He, Z. Cai, Y. Li and Q. Chen, *Eur. J. Pharm. Biopharm.*, 2008, **69**, 445–453.
33 B. Chen, J.-Z. Yang, L.-F. Wang, Y.-J. Zhang, X.-J. Lin, B. Chen, J.-Z. Yang, L.-F. Wang, Y.-J. Zhang and X.-J. Lin, *BMC Cancer*, 2015, **15**, 752.

34 U. Abdi and W. T. Al-Jamal, Submitted for publication, 2025.
35 K. Y. Hernández-Giottonini, R. J. Rodríguez-Córdova, C. A. Gutiérrez-Valenzuela, O. Peñuñuri-Miranda, P. Zavala-Rivera, P. Guerrero-Germán and A. Lucero-Acuña, *RSC Adv.*, 2020, **10**, 4218–4231.
36 A. Reisch, A. Runser, Y. Arntz, Y. Mély and A. S. Klymchenko, *ACS Nano*, 2015, **9**, 5104–5116.
37 A. Budhian, S. J. Siegel and K. I. Winey, *Int. J. Pharm.*, 2007, **336**, 367–375.
38 Y. Javadzadeh, F. Ahadi, S. Davaran, G. Mohammadi, A. Sabzevari and K. Adibkia, *Colloids Surf., B*, 2010, **81**, 498–502.
39 V. Kumar, V. Mundra and R. I. Mahato, *Pharm. Res.*, 2014, **31**, 1158–1169.
40 H. Li, Y. Fu, T. Zhang, Y. Li, X. Hong, J. Jiang, T. Gong, Z. Zhang and X. Sun, *Adv. Funct. Mater.*, 2015, **25**, 7457–7469.
41 M. Alvi, A. Yaqoob, K. Rehman, S. M. Shoaib and M. S. H. Akash, *AAPS Open*, 2022, **8**, 1–17.
42 R. Singh and J. W. Lillard, *Exp. Mol. Pathol.*, 2009, **86**, 215–223.
43 S. Fredenberg, M. Wahlgren, M. Reslow and A. Axelsson, *Int. J. Pharm.*, 2011, **415**, 34–52.
44 D. J. Hines and D. L. Kaplan, *Crit. Rev. Ther. Drug Carrier Syst.*, 2013, **30**, 257–257.
45 K. Owodeha-Ashaka, M. O. Ilomuanya and A. Iyire, *Prog. Biomater.*, 2021, **10**, 207–220.
46 M. A. U. Alam, A. Kassu and L. Kassama, 2022 ASABE Annual International Meeting, 2023, DOI: 10.13031/aim.202200474.
47 G. Kumar, S. Malhotra, N. Shafiq, P. Pandhi, G. K. Khuller and S. Sharma, *J. Microencapsulation*, 2011, **28**, 717–728.
48 I. Amjadi, M. Rabiee and M. S. Hosseini, *Iran. J. Pharm. Res.*, 2013, **12**, 623–623.
49 J. Rodrigues, M. A. Heinrich, L. M. Teixeira and J. Prakash, *Trends Cancer*, 2021, **7**, 249–264.
50 R. Francescone, H. C. Crawford and D. B. Vendramini-Costa, *Cell. Mol. Gastroenterol. Hepatol.*, 2024, **17**, 737–743.
51 D. Yang, J. Liu, H. Qian and Q. Zhuang, *Exp. Mol. Med.*, 2023, **55**(7), 1322–1332.
52 G. Shim, M.-G. Kim, D. Kim, J. Y. Park and Y.-K. Oh, *Adv. Drug Delivery Rev.*, 2017, **115**, 57–81.
53 Q. Zhou, Y. Zhou, X. Liu and Y. Shen, *Sci. Rep.*, 2017, **7**, 1–11.
54 S. Hehlgans, P. Booms, Ö. Güllülü, R. Sader, C. Rödel, P. Balermpas, F. Rödel, S. Ghanaati, S. Hehlgans, P. Booms, Ö. Güllülü, R. Sader, C. Rödel, P. Balermpas, F. Rödel and S. Ghanaati, *Int. J. Mol. Sci.*, 2018, **19**, 2485.